Biophysical *Journal*
Article

Biophysical Society

Mechanosensitive Junction Remodeling Promotes Robust Epithelial Morphogenesis

Michael F. Staddon,[1,2] Kate E. Cavanaugh,[3,4] Edwin M. Munro,[3,5] Margaret L. Gardel,[5,6,7] and Shiladitya Banerjee[1,2,8,*]

[1]Department of Physics and Astronomy and [2]Institute for the Physics of Living Systems, University College London, London, United Kingdom; [3]Department of Molecular Genetics and Cell Biology, [4]Committee on Development, Regeneration and Stem Cell Biology, [5]Institute for Biophysical Dynamics, [6]Department of Physics, and [7]James Franck Institute, University of Chicago, Chicago, Illinois; and [8]Department of Physics, Carnegie Mellon University, Pittsburgh, Pennsylvania

ABSTRACT Morphogenesis of epithelial tissues requires tight spatiotemporal coordination of cell shape changes. In vivo, many tissue-scale shape changes are driven by pulsatile contractions of intercellular junctions, which are rectified to produce irreversible deformations. The functional role of this pulsatory ratchet and its mechanistic basis remain unknown. Here we combine theory and biophysical experiments to show that mechanosensitive tension remodeling of epithelial cell junctions promotes robust epithelial shape changes via ratcheting. Using optogenetic control of actomyosin contractility, we find that epithelial junctions show elastic behavior under low contractile stress, returning to their original lengths after contraction, but undergo irreversible deformation under higher magnitudes of contractile stress. Existing vertex-based models for the epithelium are unable to capture these results, with cell junctions displaying purely elastic or fluid-like behaviors, depending on the choice of model parameters. To describe the experimental results, we propose a modified vertex model with two essential ingredients for junction mechanics: thresholded tension remodeling and continuous strain relaxation. First, junctions must overcome a critical strain threshold to trigger tension remodeling, resulting in irreversible junction length changes. Second, there is a continuous relaxation of junctional strain that removes mechanical memory from the system. This enables pulsatile contractions to further remodel cell shape via mechanical ratcheting. Taken together, the combination of mechanosensitive tension remodeling and junctional strain relaxation provides a robust mechanism for large-scale morphogenesis.

SIGNIFICANCE During development, epithelial tissues form complex structures like organs through precise spatiotemporal coordination of cell shape changes. In vivo, many morphogenetic events are driven by pulsatile cellular contractions, which are rectified to produce irreversible tissue deformations. The functional roles of these oscillatory contractions and the significance of their temporal structure remain elusive. Here, we combine theory and biophysical experiments to demonstrate that pulsed contraction acts as a mechanical ratchet to guide directed morphogenesis in epithelial tissues.

INTRODUCTION

During tissue morphogenesis and repair, individual cells dynamically alter their size and shapes in a highly coordinated fashion, resulting in tissue-scale deformations (1–3). At the single-cell level, morphogenetic forces are actively generated by dynamic actin filaments in association with myosin-II motors (4). To effect cell shape changes, active contractions generated by myosin motors must overcome both adhesion forces at cell-cell interfaces, and viscous drag from the environment (5,6). In vivo, pulses of myosin have been reported to drive cell shape changes in a cyclic fashion as a mechanical ratchet, with cell-cell junctions undergoing a series of contraction, stabilization, and relaxation (7). These pulses coordinate robust, tissue-scale deformations during apical constriction (1), where cell apical areas successively shrink to drive bending of the epithelial tissue, or during *Drosophila* germband extension (2), where cell-cell junctions contract and intercalate to elongate the tissue.

Submitted June 17, 2019, and accepted for publication September 24, 2019.

*Correspondence: shiladitya.banerjee@ucl.ac.uk or shiladtb@andrew.cmu.edu

Editor: Stanislav Shvartsman.

https://doi.org/10.1016/j.bpj.2019.09.027

Although myosin-driven contraction pulses are ubiquitous in morphogenetic events, the functional roles of the amplitude or the frequency of contractions remain unknown.

From a mechanistic perspective, tissue cells must be capable of resisting large deformations to maintain their mechanical integrity while being able to dissipate stresses to undergo remodeling. It remains poorly understood how cells modulate their elastic and viscous properties to respond and adapt to mechanical stresses. A number of different experimental techniques and model systems have been used to probe the viscoelastic properties of epithelial cells. Rheological studies on suspended epithelial monolayers (8) have shown that stress dissipation in strained tissues is controlled by cell divisions or actomyosin turnover (9,10). Optical tweezers have been used to probe the mechanical response of cell-cell junctions under short timescale forces, where they respond elastically (6). At longer timescales, junctions undergo permanent length changes in response to myosin-generated forces (11). Despite the growing evidence for active remodeling of junction mechanical properties (12,13), most theoretical models for epithelial mechanics, such as the vertex model (14–16), cellular Potts model (17,18), or continuum models (19–21), assume constant interfacial tensions and cell contractility. Although some recent models attempt to model junctional mechanics (9,22–25), these have not been directly tested in experiments at the scale of individual cell junctions.

In this study, we combine theory and biophysical experiments to propose a new model for epithelial cell shape control via mechanosensitive remodeling of junctional tension and strain. Using optogenetic control of RhoA (26), the upstream regulator of actomyosin contractility, we study how adherens junction length responds to acute tension changes of varied amplitude and duration. We find that epithelial cell junctions behave elastically in response to short timescale activations of RhoA. Under longer timescale activation of RhoA, junction contraction eventually stalls and does not recover to its initial length upon RhoA removal. The existing vertex-based models for epithelial mechanics are unable to capture these results, with junctions displaying either purely viscous or elastic responses, regardless of the magnitude of applied stress. We thus propose a new model in which junctional tension remodels irreversibly only when deformed above a threshold value. In addition, junctions undergo continuous strain relaxation to allow for the removal of mechanical memory. Taken together, thresholded tension remodeling and continuous strain relaxation captures the mechanical behavior of intercellular junctions under stress and predicts mechanical ratcheting under episodic activations of contractility in quantitative agreement with experimental data. Our model provides a potential new understanding of pulsatile contractions that have been widely observed during morphogenesis in vivo (1,7). In particular, pulsatile contraction enables epithelial junction shortening further beyond the limit of a single prolonged contraction pulse.

MATERIALS AND METHODS

Optogenetic experiments

We use optogenetic control of RhoA to induce contractions at epithelial cell junctions (Fig. 1). Caco-2 cells stably expressing the TULIP optogenetic system (27) were plated atop polymerized collagen gels coating a four-well chamber (Ibidi Chambers, Gräfelfing, Germany) at a final concentration of 2 mg/mL. Cells were plated at least 2 days before optogenetic experiments to ensure a polarized and mature epithelial monolayer. Cell-cell junctions were delineated with CellMask Deep Red plasma membrane stain (Molecular Probes, Life Technologies, Carlsbad, CA). Junctions expressing the constructs required for visible optoGEF recruitment were chosen for activation. Junctions were illuminated by a 405 nm laser for 1000 ms before each image acquisition every 35 s (Fig. 1). Regions were drawn in Metamorph (Molecular Devices, Sunnyvale, CA) and manually adjusted in real time to ensure the blue light was restricted to the activated junction. Junction lengths were manually measured in Fiji software using the segmented line tool. A Mosaic digital micromirror device (Andor Technology, Belfast, UK) was used for optogenetic recruitment using a 405-nm laser. A Nikon Ti-E (Nikon, Tokyo, Japan) with a Yokogawa CSU-X confocal scanning head (Yokogawa Electric, Tokyo, Japan) and laser merge model with 491, 561, and 642 nm laser lines (Spectral Applied Research, Ontario, Canada) was used to image cells. The objective used was a 60× 1.49 NA ApoTIRF oil immersion objective (Nikon) or a 60× 1.2 Plan Apo water (Nikon) objective.

Vertex-based model for epithelium

To develop a mechanistic understanding of junctional length regulation in response to applied stresses, we first implemented a vertex-based model (28), which has been widely used to model epithelial tissue remodeling (24,29), wound healing (15,30,31), collective motility (32), tissue growth (33,34), and cell-matrix adhesions (35). In the commonly used two-dimensional vertex models (14,28,34), the geometry of each cell is defined by a polygon, with cell-cell junctions represented by linear edges and three-way junctions by vertices (Fig. 2 *a*). The tissue mechanical energy is given by:

$$E = \frac{1}{2}\sum_{\alpha} K(A_\alpha - A_0)^2 + \frac{1}{2}\sum_{\alpha} \Gamma(P_\alpha - P_0)^2, \qquad (1)$$

where the first term represents three-dimensional incompressibility of cells with K as the height elastic constant, A_α is the planar area of cell α, and A_0 is the preferred area. The second term in Eq. 1 results from a combination of actomyosin contractility in the cell cortex and intercellular adhesions, where Γ is the elastic constant for contractility, P_α is the perimeter of cell α, and P_0 is the preferred perimeter. The geometric parameters of the vertex model define a target shape index, $p_0 = P_0/\sqrt{A_0}$, which controls the mechanical properties of the tissue (14,29). In particular, the tissue behaves like an elastic solid for $p_0 < 3.81$, whereas it flows like a viscous liquid for $p_0 > 3.81$ (14). In the overdamped limit, motion for each vertex i is governed by:

$$\mu \frac{dx_i}{dt} = -\frac{\partial E}{\partial x_i}, \qquad (2)$$

where μ is the drag coefficient, and x_i is the position of vertex i. The tension Λ_{ij} on edge ij, connecting vertices i and j, is given by $\Lambda_{ij} = \partial E/\partial L_{ij}$, where L_{ij} is the length of edge ij. For the Hamiltonian in Eq. 1, $\Lambda_{ij} = \sum_\alpha \Gamma(P_\alpha - P_0)$, where the sum is over all cells containing the edge ij. To simulate the effect of time-dependent myosin induced contractions on edge ij, we apply an additional tension $\Lambda_a = \Gamma_a L_{ij}/2$, where Γ_a represents the product of myosin density and the force exerted by each myosin unit.

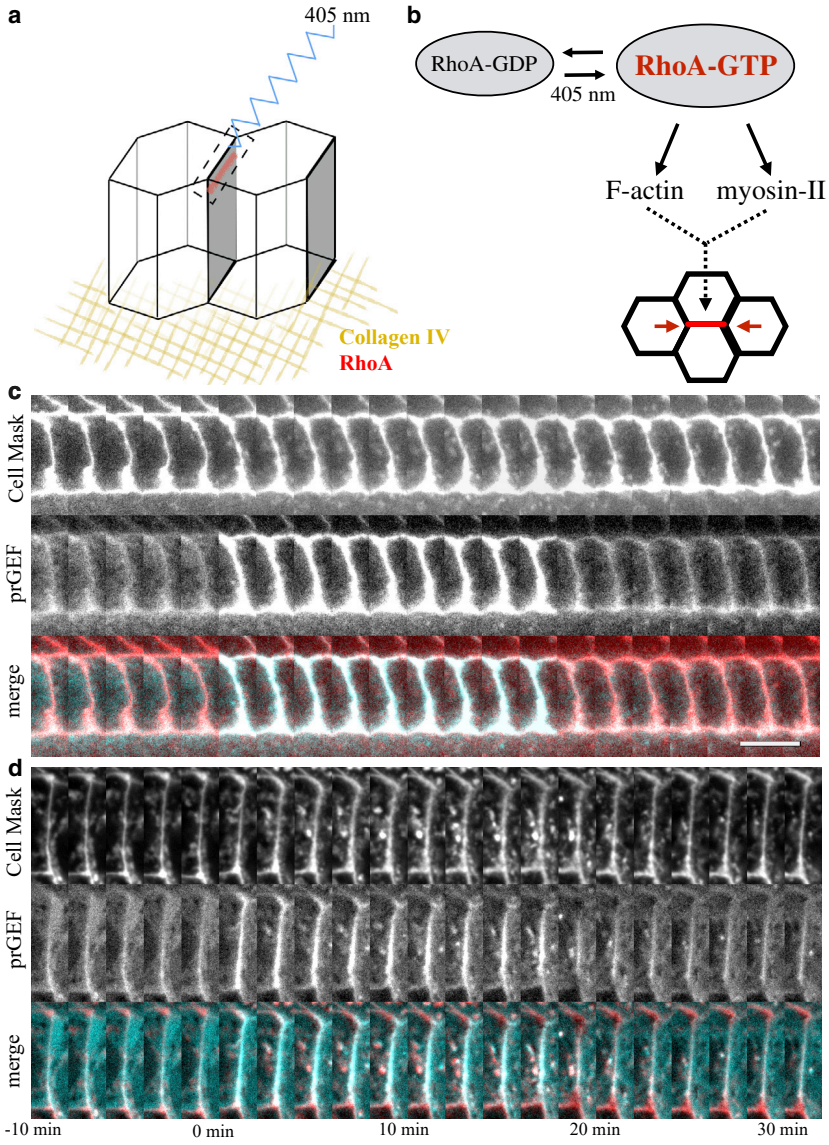

FIGURE 1 Optogenetic control of RhoA. (*a*) Schematic of optogenetics experiments. Caco-2 cells expressing the TULIP optogenetic system are plated on a polymerized collagen gel. A target junction is illuminated by a 405-nm laser, activating RhoA and inducing actomyosin contraction. (*b*) Schematic of the Rho pathway. (*c* and *d*) Time lapse images for a 20-min activation at 100% light intensity (*c*) and at 50% light intensity (*d*). The images show, from top to bottom, CellMask Deep Red, prGEF, and merged (CellMask *Deep Red* in *red*, prGEF in *cyan*). Time interval between successive image frames is 2 min in each row of (*c*) and (*d*). Scale bars, 5 μm. To see this figure in color, go online.

Model implementation

The model is simulated using Surface Evolver (36). In simulations, we nondimensionalize force scales by $KA_0^{(3/2)}$ and length scales by $\sqrt{A_0}$, setting $K = 1$ and $A_0 = 1$. Thus, Eq. 1 becomes:

$$E = \frac{1}{2}\sum_{\alpha}(A_\alpha - 1)^2 + \frac{1}{2}\sum_{\alpha}\Gamma(p_\alpha - p_0)^2. \qquad (3)$$

A round tissue of 50 cells, with stress-free boundary conditions, is first relaxed so that the simulations begin at mechanical equilibrium. Then 15 different cell edges, excluding edges on boundary cells, are randomly selected for activation of contractility. After each activation, the tissue is reset to the equilibrium state and then the next cell edge is activated. We simulate a range of values of p_0 to test the response of both solid and fluid tissues. The value of contractility, Γ, is taken from Farhadifar et al. (34), and we use a constant value for friction coefficient, μ (Table 1). For each value of p_0, we choose Γ_a such that the normalized junction length after a 20-min activation is the same as in the experiments (Fig. 2 *b*). Any cell edge that contracts below a critical length, $L_{T_1} = 0.05$, and would decrease in length over the next time step, undergoes a T_1 transition. Here, the cells rearrange and the contracted edge is replaced by a perpendicular edge of the same length, following which the edge tension is set to the initial value.

RESULTS AND DISCUSSION

Viscoelastic behavior of epithelial cell junctions

Upon application of contractile stress along chosen cell edges over a finite duration (Fig. 2 *b*; Materials and Methods), the vertex model predicts that cell junctions immediately contract while eventually slowing down for a tissue in the solid state (Fig. 2, *b* and *c*). After the activation period, the elastic tissue recoils back to its original length, whereas a fluid tissue exhibits no recoil and remains permanently deformed. In the fluid state (Fig. 2, *b* and *d*), cells can freely adjust their area and perimeter in response to applied

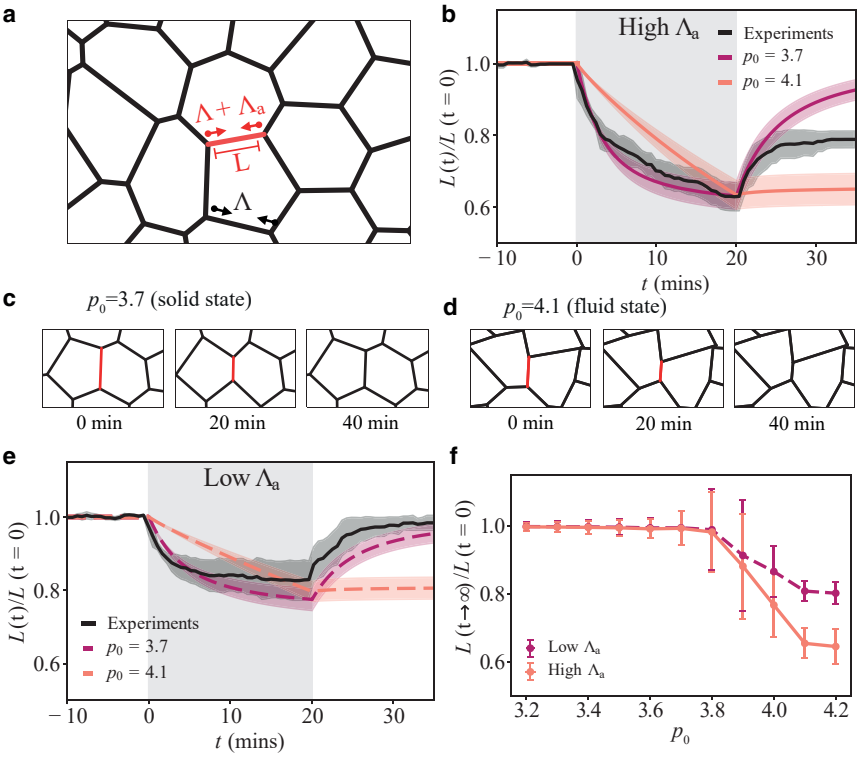

FIGURE 2 Elastic and viscous response of intercellular junctions in the vertex model. Results shown are obtained using the traditional vertex model (Eq. 1). (*a*) Schematic image of the vertex model. The red edge represents the junction under applied tension, Λ_a. (*b*) Normalized junction length over time, during and after a 20-min activation for high applied tension. Gray shaded region indicates the activation period. Red curve: $p_0 = 3.7$, orange curve: $p_0 = 4.1$, black curve: experimental data for 20-min activation of RhoA. Solid lines show the mean trend, and shaded area represents SD (simulations: n = 15, experiments: n = 6). (*c* and *d*) Simulation images of a junction before, during, and after a 20-min activation, for (*c*) a solid tissue, $p_0 = 3.7$, and (*d*) a fluid tissue, $p_0 = 4.1$. (*e*) Normalized junction length over time, during and after a 20-min activation for high applied tension (simulations: n = 15, experiments: n = 4). (*f*) Normalized final junction length against preferred shape index p_0, for high and low values of applied tension, Λ_a (n = 15). For parameters, see Table 1. To see this figure in color, go online.

stress, resulting in edges under no tension. Junctions in a fluid tissue can contract at no energy cost (14), with the neighboring cells adjusting their shapes, resulting in permanent changes in junction length after applied contraction (Fig. 2 *d*). By contrast, cell junctions are under tension for a solid tissue, stable to small mechanical perturbations. Consequently, contracted edges return to their original lengths after the activation period (Fig. 2, *b* and *c*).

To test the predictions of the vertex model, we use optogenetic control of RhoA in Caco-2 cells (26,27,37,38). By targeting light at chosen cell-cell junctions, we are able to increase actomyosin contraction in a highly localized region (Fig. 1, *a* and *b*) (Materials and Methods). Applying a 20-min activation, we observe a rapid contraction of the junction to 63 ± 4% of its initial length (Figs. 1 *c* and 2 *b*). After RhoA activation, the junction recoils and recovers to 78 ± 2% of its initial length. This indicates a viscoelastic response of the junction, with elastic response on short timescales and viscous behavior, by permanent length changes, on longer timescales. These data stand in contrast to the predictions of the vertex model. Furthermore, by tuning the light intensity, we are able to control the amount of contractile stress on the junction. When applying 50% of the light intensity, the initial junction contraction rate drops by half; the junction contracts 14 ± 3% over 5 min vs. 23 ± 3% at full light intensity (Fig. 1, *c* and *d*). This is followed by a slow phase of contraction that eventually stalls (Fig. 2 *e*). After the activation period, the junction recoils back to its original length, akin to an elastic material.

To simulate low light activation of RhoA, we applied half the active tension Λ_a in simulations. As before, we find an elastic response of the junction for $p_0 < 3.81$, and no recoil in the fluid state (Fig. 2 *e*). Testing several other values of the preferred shape index p_0, we observe no deformation for the solid state at both high and low values of Λ_a (Fig. 2 *f*). As p_0 is increased to values >3.81 (fluid phase), we observe permanent junction deformation for high Λ_a. In contrast to experiments, where deformation requires a threshold amount of stress, low Λ_a still produces a permanent deformation, which is at least 50% of the strain at high Λ_a. Thus, the vertex model is unable to capture the viscoelastic response of cell junctions under high contractile

TABLE 1 Vertex Model Parameters

Parameter	Value
Contractility, Γ	0.04
Friction Coefficient, μ	0.25 min
$\Gamma_a(p_0 = 3.2)$	0.1416
$\Gamma_a(p_0 = 3.3)$	0.1206
$\Gamma_a(p_0 = 3.4)$	0.0994
$\Gamma_a(p_0 = 3.5)$	0.0784
$\Gamma_a(p_0 = 3.6)$	0.0576
$\Gamma_a(p_0 = 3.7)$	0.0374
$\Gamma_a(p_0 = 3.8)$	0.0216
$\Gamma_a(p_0 = 3.9)$	0.0138
$\Gamma_a(p_0 = 4.0)$	0.0110
$\Gamma_a(p_0 = 4.1)$	0.0106
$\Gamma_a(p_0 = 4.2)$	0.0104

Parameters are for Fig. 2.

stress. Our data also stand in contrast to (11), where cell-cell junctions are modeled as Maxwell viscoelastic elements. Under this model, even low contractile stresses should continuously shorten the junction.

Strain-dependent junction remodeling captures adaptive junction length changes

Our experimental data show that irreversible junction deformations occur only for sufficiently high amplitudes of contraction, suggesting a thresholded viscoelastic response of intercellular junctions. To this end, we modify the existing vertex model to incorporate irreversible junctional length remodeling above a threshold strain.

We adapt the vertex model to treat each cell edge as an elastic spring with spring constant Y, and a dynamically changing rest length, L_{ij}^0 (Fig. 3 *a*). The rest length remodels according to:

$$\frac{1}{L_{ij}^0}\frac{dL_{ij}^0}{dt} = \begin{cases} k_L \varepsilon_{ij} & \text{if } \varepsilon_{ij} > \varepsilon_c \,, \\ 0 & \text{if } -\varepsilon_c \le \varepsilon_{ij} \le \varepsilon_c \,, \\ k_L \varepsilon_{ij} & \text{if } \varepsilon_{ij} < -\varepsilon_c \,, \end{cases} \tag{4}$$

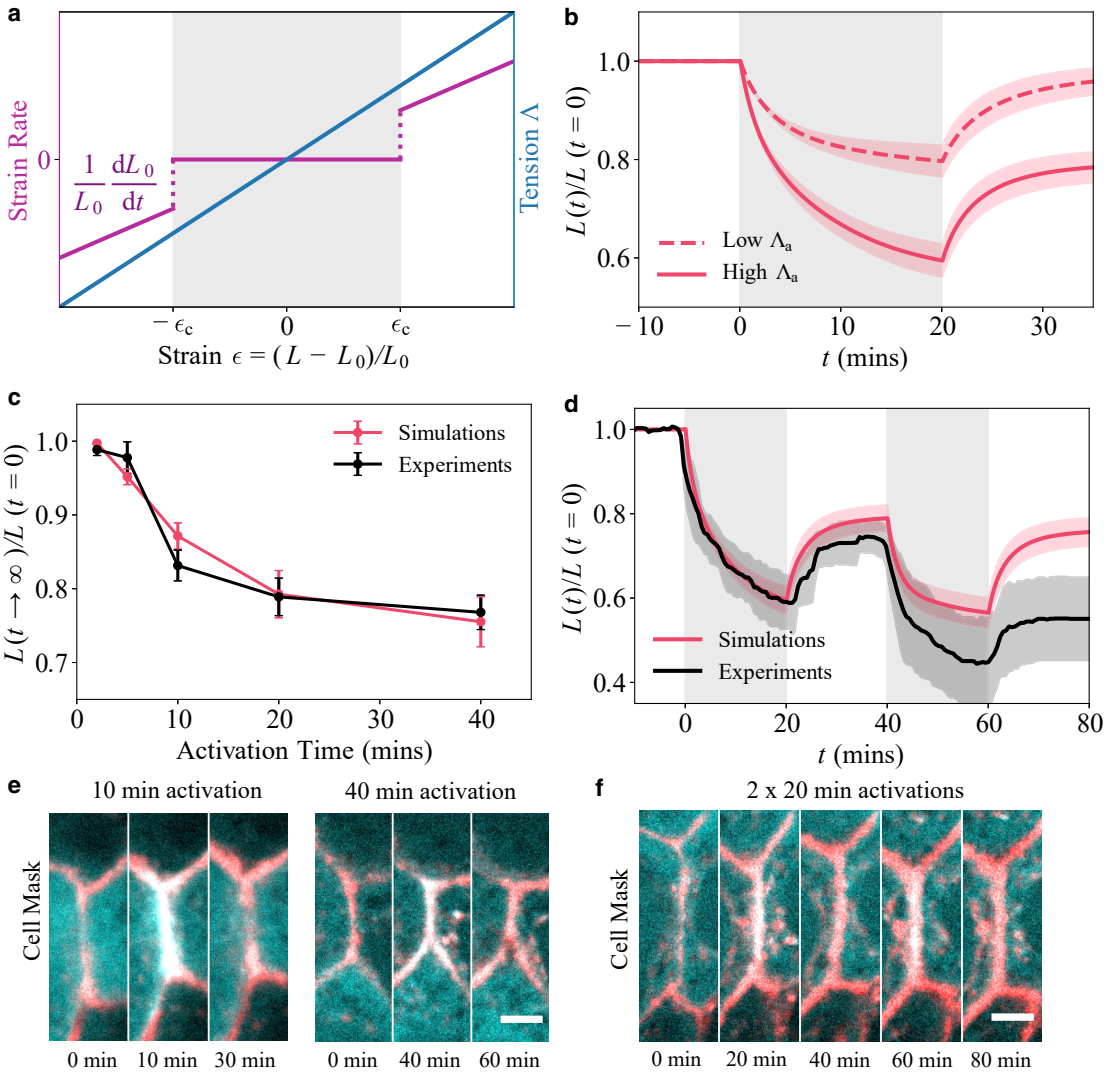

FIGURE 3 Threshold strain is required to trigger junction length remodeling. Results shown are obtained using the active spring model (Eq. 4). (*a*) Rate of change in rest length, $\dot{L}_0/L_0$, and edge tension Λ, as a function of junction strain ε. (*b*) Model predictions for normalized junction length over time for a 20-min step pulse of contraction, for high (Λ_a) and low ($\Lambda_a/2$) values of applied tension. Solid and dashed lines show the mean, and shaded areas represent SD (n = 15). (*c*) Comparing experimental data and model predictions for (normalized) final junction length versus contraction time. (Simulations: all times, n = 15. Experiments: 2 min, n = 5; 5 min, n = 9; 10 min, n = 3; 20 min, n = 6; 40 min, n = 3). (*d*) Normalized junction length versus time for two consecutive 20-min contraction pulses for experiments and simulations (simulations: n = 15, experiments: n = 3). (*e*) Time lapse images (*left* to *right*) before activation, at the end of activation, and after activation for 10- and 40-min activations. (*f*) Time lapse images (*left* to *right*) before activation, at the end of the first activation, before the second activation, at the end of the second activation, and after both activations, for two 20-min activations with a 20-min rest in between. Scale bars, 5 μm. For parameters see Table 2. To see this figure in color, go online.

where $\varepsilon_{ij} = L_{ij}/L_{ij}^0 - 1$ is the strain on edge ij, ε_c is a critical strain beyond which rest length remodeling is triggered, and k_L is the rate of remodeling. The idea of rest length remodeling was first introduced by Odell et al. (39), who treated actomyosin bundles at cell junctions as elastic springs, whose rest length reduces to a shorter value beyond a threshold amount of contraction. Rest length remodeling is a natural consequence of actomyosin networks deforming with turnover, when strained network elements are replaced by unstrained ones (40). The tension on each edge is given by $\Lambda_{ij} = Y\varepsilon_{ij}$, such that the mechanical energy of the tissue is:

$$E = \frac{1}{2}\sum_{\alpha} K(A_\alpha - A_0)^2 + \frac{1}{2}\sum_{ij}\Lambda_{ij}\varepsilon_{ij}. \quad (5)$$

Parameters for this "active spring model" (Table 2) are fit to experimental data by minimizing the mean-square difference between the normalized junction length in simulations and the mean length in experiments the 2-, 5-, 10-, 20-, and 40-min (n = 3) activations and two consecutive 20-min activations (Fig. 3 *d*). We compute the fitting error as:

$$\text{Error} = \frac{1}{6}\sum_{a}\sum_{ij}\frac{1}{T_a}\int_0^{T_a}\left(\left\langle\frac{L^a_{\text{exp}}(t)}{L^a_{\text{exp}}(0)}\right\rangle - \frac{L^a_{ij}(t)}{L^a_{ij}(0)}\right)^2 dt, \quad (6)$$

where a indicates the different activation experiments described above, T_a is the total experimental time, ij indicates the activated junction in the simulation, and $\langle L^a_{\text{exp}}(t)/L^a_{\text{exp}}(0)\rangle$ is the normalized junction length averaged over all experiments. The Simplex (or Nelder-Mead) algorithm is used to minimize the fitting error.

This model predicts that junction contraction is biphasic upon activation of a single contraction pulse of magnitude Λ_a. For high Λ_a, junction length shortens quickly, and then begins to slow down and eventually stalls (Fig. 3 *b*). Once the strain in the junction exceeds ε_c, the junction rest length begins to remodel and becomes shorter. After the activation period, the junction recoils, but a shorter rest length leads to an increased tension in the edge, resulting in a shorter final length of the junction (Fig. 3 *b*). When applying half the tension Λ_a, the critical strain ε_c is never reached. As a result, the rest length remains unchanged, and the junction recoils back to its initial length after activation (Fig. 3 *b*). Thus, very short timescale activations are unable to contract the junction beyond the critical strain, leading to elastic response and perfect length recovery (Fig. 3 *c*). Longer timescale activations are required to trigger junctional remodeling. However, remodeling slows down with increasing activation period, thereby limiting the amount of length shortening as observed in experiments (Fig. 3, *c* and *e*).

TABLE 2 Parameters for Active Spring Model of Epithelial Cell Junctions

Parameter	Value
Rest length remodeling rate, k_L	0.227 min^{-1}
Critical strain, ε_c	0.091
Spring constant, Y	0.280
Applied contractility, Γ_a	0.337
Friction, μ	5.502 min

As the final length saturates to $82 \pm 5\%$ of its initial value, irrespective of the magnitude of Λ_a or the activation period, we investigated if a second contraction pulse could overcome this length saturation. In optogenetic experiments, a second 20-min activation pulse of RhoA (with a 20-min rest in between) leads to ratcheted contraction (Fig. 3, *d* and *f*). Junction length after the second contraction drops to 80% of its value after the first contraction. However, this behavior is not reproduced by our model for thresholded junctional length remodeling. After the second activation, the junction length recoils back to its value after the first activation (Fig. 3 *d*).

To understand the mechanistic origin of these results, we compute the edge tension and strain during the pulsatile stress protocol (Fig. 4 *a*). During the first activation period, the edge is compressed, resulting in a negative tension acting to expand the junction length. As the strain drops below the critical value, $-\varepsilon_c$, the rest length begins to remodel at a rate proportional to the strain. This results in rest length shortening, which brings back the strain to its critical value, $-\varepsilon_c$, at which tension and strain remodeling stops. After the removal of exogenous tension, the junction length recoils beyond the rest length, resulting in a positive tension and a permanently strained (shortened) junction (Fig. 4 *a*). During the second activation, the junction contraction again stalls at the fixed point $\varepsilon = -\varepsilon_c$, and the rest length is unable to remodel further. Because tension is proportional to strain, the critical strain determines the maximal steady-state tension possible, $\Lambda_{\text{max}} = Y\varepsilon_c$. Above this tension magnitude, the rest length will remodel until strain reaches the critical value. Due to the invariance in Λ_{max}, we obtain the same final edge length in the model after any number of activations.

For ratcheted contractions to occur, cell junctions must continuously relax strain to remove mechanical memory, i.e., junctions must overcome their mechanical energy barriers and not get stuck in a local energy minimum. To understand the underlying physics, we constructed an effective medium model for the cell junctions (Fig. 4 *b*-top). Here we treat forces from the neighboring cells as a spring-like restoring force, whereas the junction acts like a Maxwell viscoelastic material that requires a threshold strain for the viscous element to remodel. The energy of this effective system is given by:

$$E = \frac{Y}{2}\left(\frac{L}{L_0} - 1\right)^2 + \frac{k}{2}(L - L_i)^2 + \Lambda_a L, \quad (7)$$

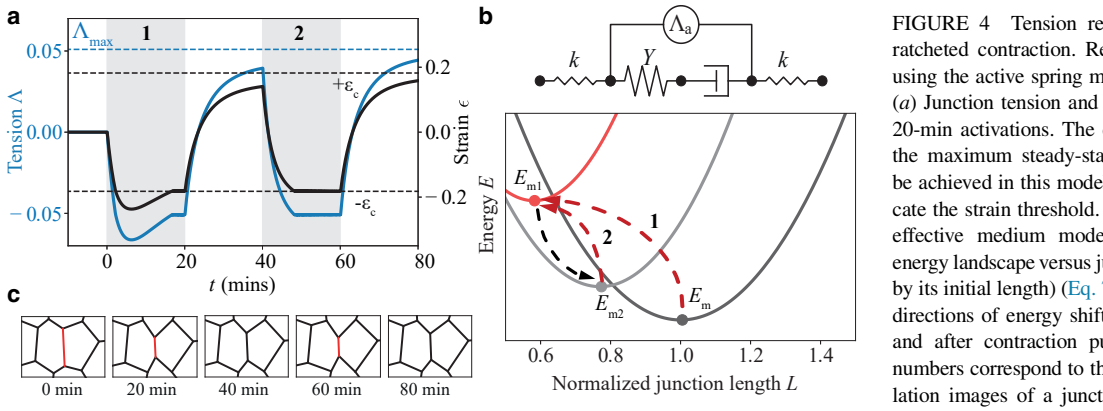

FIGURE 4 Tension remodeling is essential for ratcheted contraction. Results shown are obtained using the active spring model for junctions (Eq. 4). (*a*) Junction tension and strain versus time for two 20-min activations. The dashed blue line indicates the maximum steady-state tension, $\Lambda_{\max}$ that can be achieved in this model. Dashed black lines indicate the strain threshold. (*b*) Top: Schematic of the effective medium model. Bottom: Dynamics of energy landscape versus junction length (normalized by its initial length) (Eq. 7). The arrows indicate the directions of energy shifts during contraction (*red*) and after contraction pulse removal (*gray*). The numbers correspond to the pulse number. (*c*) Simulation images of a junction over time during two consecutive contractions, showing no ratcheting. To see this figure in color, go online.

where L is the current junction length, L_i is the initial length, and L_0 is the junction rest length. The first term represents the harmonic restoring force from the junction, the second term describes the spring-like restoring force from neighboring junctions with a spring constant k, and the final term represents the applied tension $\Lambda_a = \Gamma_a L/2$. Junction rest length remodels according to Eq. 4. Before the activation of contractility, $L = L_i = 1$, as defined by the minimum of the energy functional, E_{m} (Fig. 4 *b*).

During the first activation, $\Lambda_a \neq 0$ and the rest length L_0 shortens. This shifts the energy landscape, which now has a new minimum, E_{m1}, defining the contracted junction length (Fig. 4 *b*)

$$L_{\mathrm{m1}} \approx L_i \frac{1+\sqrt{1+4\Lambda_{\max}(1-\varepsilon_c)(1+\Gamma_a/k)/kL_i}}{2(1+\Gamma_a/k)}. \quad (8)$$

After the first activation, the energy minimum shifts to a higher value, E_{m2}, due to junction recoil. The new steady-state junction length is given by

$$L_{\mathrm{m2}} \approx \frac{L_i}{2}\left(1+\sqrt{1-4\Lambda_{\max}(1+\varepsilon_c)/kL_i}\right). \quad (9)$$

As subsequent contraction pulses are unable to change the rest length, the steady-state length of the junction between the minima (L_{m1},E_{m1}) and (L_{m2},E_{m2}) (Fig. 4 *b*). Therefore, ratcheting behavior is not programmed in this model. For the junction to contract further, an increase in edge tension is required above its maximal possible value, $\Lambda_{\max} = Y\varepsilon_c$ (Fig. 4 *a*).

Mechanosensitive tension remodeling and continuous strain relaxation promotes directed morphogenesis

In order to describe the mechanical behavior of cell junctions in response to time-dependent contractile activity, we developed a model where the edge tension is dynamically remodeled depending on the junctional strain. In this model, the rest length of each edge, L_{ij}^0, remodels at a rate k_L to match the current junction length, allowing for continuous strain relaxation (Fig. 5 *a*):

$$\frac{1}{L_{ij}^0}\frac{dL_{ij}^0}{dt} = k_L \varepsilon_{ij}. \quad (10)$$

If the strain in the junction exceeds a threshold magnitude, ε_c, then the tension begins to remodel:

$$\frac{d\Lambda_{ij}}{dt} = \begin{cases} -k_e\left(L_{ij}-L_{ij}^0\right) & \text{if } \varepsilon_{ij} > \varepsilon_c, \\ 0 & \text{if } -\varepsilon_c \le \varepsilon_{ij} \le \varepsilon_c, \\ -k_c\left(L_{ij}-L_{ij}^0\right) & \text{if } \varepsilon_{ij} < -\varepsilon_c, \end{cases} \quad (11)$$

where k_e and k_c are the rates of tension remodeling under junction extension or contraction, respectively (Fig. 5 *a*). Thus, if an edge undergoes a large and rapid contraction, the tension will begin to increase and the junction will remain irreversibly shortened. Parameters are fit by minimizing the error in Eq. 6. (Table 3).

An effective medium model for this system can be described by the energy function:

$$E = (\Lambda+\Lambda_a)L + \frac{1}{2}k(L-L_i)^2, \quad (12)$$

where the first term represents the total tension in the junction, whose dynamics are described by Eq. 11. Applying consecutive pulses of contractions would repeatedly increase the edge tension, and shift the steady-state junction length $L = (L_i - \Lambda/k)/(1+\Gamma_a/k)$ (given by the minimum of E) to successive lower values (Fig. 5 *b*). This would result in successive reductions in the final junction length. Note that tension remodeling alone is not adequate to capture the experimental data. Without rest length remodeling, there is no strain relaxation. As a result, an increased tension would rapidly contract cell edges without limit, leading to their eventual collapse.

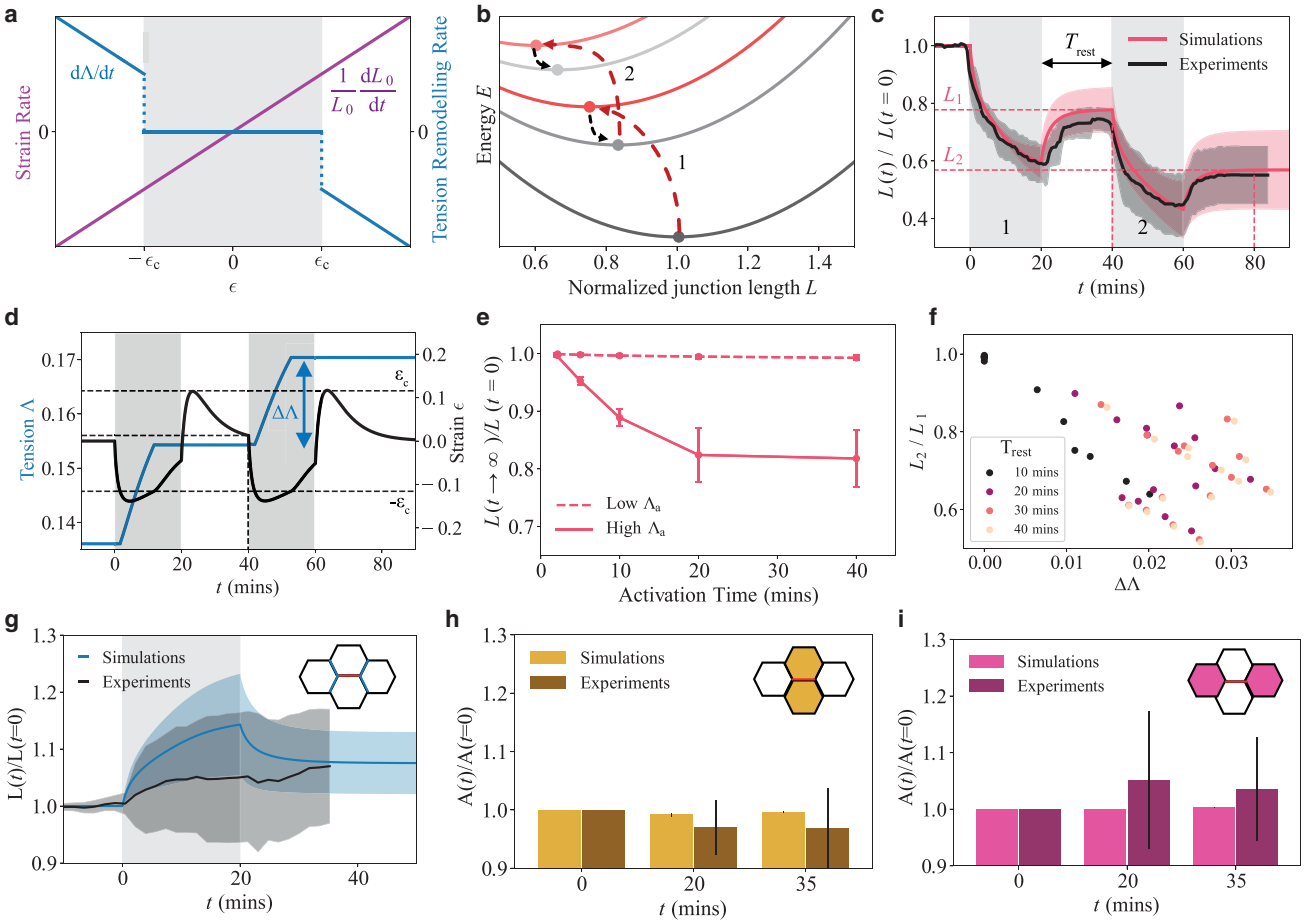

FIGURE 5 Mechanosensitive tension remodeling promotes ratcheted contractions. Results shown are obtained using the tension remodeling model (Eqs. 10 and 11) (*a*) Model for tension remodeling: rate of change in rest length, $\dot{L}_0/L_0$, and rate of change in tension, $\dot{\Lambda}/L_0$, as a function of the junctional strain ϵ. (*b*) Junction energy landscape in the tension remodeling model, as a function of normalized junction length (Eq. 12). (*c*) Normalized junction length for two successive 20-min contraction pulses, with a 20-min rest period. Solid curves show the mean trend, and shaded areas represent SD (n = 15). (*d*) Dynamics of junction tension and strain, for two successive 20-min contraction pulses. (*e*) Normalized junction length versus contraction time, for high and low values of Λ_a (n = 15). (*f*) Length ratio L_2/L_1 versus the change in tension $\Delta\Lambda$ between two consecutive 20-min contraction pulses, at different values of T_{rest}. Each point represents a different simulation. (*g*) Normalized shoulder junction length (blue *edges* in the *inset*) for a 20-min activation (simulations: n = 60, experiments: n = 11). (*h* and *i*) Normalized cell areas at different time points during a 20-min activation for adjacent cells (*h*), shown in yellow, and border cells (*i*), shown in pink (simulations: n = 30, experiments: n = 13). Error bars represent SD. For parameters, see Table 3. To see this figure in color, go online.

Ratchet-like contractions

We find that the combination of continuous strain relaxation (Eq. 10) and thresholded tension remodeling (Eq. 11) is sufficient to capture the experimentally observed mechanical behavior of epithelial junctions, as well as ratcheted contractions upon episodic activation of contractility. In agreement with experimental data (Fig. 3 *d*), the junction shrinks to $\sim 80\%$ of its initial length after the first contraction, whereas after the second contraction pulse, the normalized junction length is 70%, roughly 85% of its length after the first pulse (Fig. 5 *c*). During each activation, the strain drops below the critical strain and tension is irreversibly increased, allowing the junction length to shrink further than after the first activation (Fig. 5 *d*). Unlike the model with purely rest length remodeling (Fig. 4), combination of tension and rest length remodeling allows the junctional strain to relax back to zero after the removal of exogenous tension (Fig. 5 *d*). Continuous strain relaxation allows for the removal of mechanical memory, which is crucial for promoting contraction below the critical strain during each successive pulse.

TABLE 3 Tension Remodeling Model Parameters

Parameter	Value
Rest length remodeling rate, k_L	0.189 min^{-1}
Critical strain, ϵ_c	0.116
Initial tension, Y	0.136
tension remodeling rate, k_c	0.027 min^{-1}
tension remodeling rate, k_e	0.000 min^{-1}
Applied contractility, Γ_a	0.065
Friction, μ	0.636 min

Because very short timescale activations are unable to trigger tension remodeling, the junctions recoil back to their original length, in line with experimental data (Fig. 5 *e*). By contrast, longer activation periods increase the amount of tension remodeling and junction length shortening. For single activations, junction shortening stalls for very long activation periods (>20 min), in agreement with experimental data (Fig. 3 *c*). Thus, ratcheting provides a mechanism to further shorten junctions past the single contraction limit. Applying a lower tension is incapable of sufficiently straining the junction, and therefore a combination of high Λ_a and long activation period is required for junctional remodeling (Fig. 5 *e*).

We quantified the efficiency of ratcheting by computing the ratio of lengths before and after the second activation period (Fig. 5 *c*). For a given rest period T_{rest} between the activations, we define L_1 as the length before the second activation, and L_2 as the length T_{rest} minutes after the second activation. For different values of T_{rest}, we compare the ratio L_2/L_1 to the change in tension $\Delta\Lambda$ after the second activation (Fig. 5 *d*). We find a robust negative correlation between L_2/L_1 and $\Delta\Lambda$ (Fig. 5 *f*). A longer T_{rest} allows the junctional strain to relax to zero when $\Lambda_a = 0$. Consequently, we obtain a more effective ratchet, with a higher $\Delta\Lambda$ and a lower L_2/L_1 (Fig. 5 *f*).

In this model, we have assumed that irreversible junction length changes are due to remodeling of single cell-cell junctions. However, morphogenetic cell shape changes can also occur via contraction of the entire cell area through cycles of apical constriction (1). To test this, we measured the lengths of the shoulder junctions (Fig. 5 *g*), the area of cells adjacent to the junction (Fig. 5 *h*), and bordering the junction (Fig. 5 *g*). If cells apically constrict after optogenetic activations, we would expect that the cells adjacent to the activated junction would shrink in area, contracting the shoulder junctions, whereas those bordering the junction remain at a constant area. In our experiments, the shoulder junctions show a $7 \pm 10\%$ increase in length after an activation (1 sample *t*-test: $n = 27$, $t = 8.10$, $p < 0.001$) (Fig. 5 *g*). When we measure the adjacent cell and border cell areas, we find that neither show a significant change in length. The adjacent cells decrease in area by $3 \pm 7\%$ (1 sample *t*-test: $n = 13$, $t = -1.61$, $p = 0.13$) (Fig. 5 *h*), and the border cells increase in area by $4 \pm 9\%$ (1 sample *t*-test: $n = 13$, $t = 1.33$, $p = 0.208$) (Fig. 5 *i*). Our simulations capture these results, with a similar increase in shoulder junction length, and changes in area of less than 1% after activations (Fig. 5, *g–i*). Thus, we rule out remodeling of apical medial actomyosin as a contributor to the irreversible junction length changes.

Our data suggest that junctions under large stresses undergo an irreversible tension remodeling, stabilizing the junction into a shorter length. We strongly suspect that changes in junction tension would also require changes in junctional Rho levels, which, through its downstream effectors control levels of actin and myosin-II. However, how the endogenous RhoA levels at junctions is variably maintained or modulated remain an open area of research. First, our experimental data indicates the contraction is occurring heterogeneously, with only 25% of the junction contracting. Thus, one plausible scenario is that contraction of a local region of junction coincides with pinching off and internalization of that region via endocytosis (27). Finally, the continuous strain remodeling may arise from turnover of junctional actomyosin and E-cadherin, similar to recent reports in Iyer et al. (12). We believe that junctions under high compressive strain undergo an increase in E-cadherin turnover, which reduces adhesion and thus increases junctional tension.

Convergence-extension movements

To test the effectiveness of mechanical ratcheting for tissue-scale deformation, we applied our model of mechanosensitive tension remodeling (Eqs. 10 and 11), to simulate convergent-extension movements. Convergent-extension is a widespread mode of tissue morphogenesis, where a tissue segment converges along one axis as an oscillatory ratchet, while extending along the other axis via cell rearrangements (41). To simulate convergent-extension, we generated a colony of hexagonal cells and applied a time-dependent tension, Λ_a, along its horizontal edges, in five 40-min pulses (Fig. 6, *a* and *b*; Videos S1, S2, S3). Once a cell edge contracts below a threshold length, L_{min}, it undergoes an intercalation event resulting in cell neighbor exchanges. During activations of contractility, the tissue converges horizontally, and extends vertically via cell rearrangements, resulting in a higher aspect ratio shape (Fig. 6, *a* and *b*). During the rest period between activations, the tissue remains in a deformed state due to irreversible tension remodeling. By allowing longer rest periods between successive contractions, the amount of tension remodeling increases, resulting in a higher aspect ratio structure (Fig. 6 *c*; Table 4) with more cell rearrangements (Fig. 6 *a*). Thus, our model for tension remodeling is sufficient to capture tissue-scale deformations via ratcheted contractions, as commonly observed in morphogenesis.

CONCLUSIONS

Pulsatile regulatory dynamics are recurrent in cells and enable diverse cellular functions through independent control of pulse frequency, amplitude, and duration (42). In development, pulses of actomyosin have been shown to coordinate epithelial cell shape changes and mechanical stability (1,7,43–45). However, the functional roles of actomyosin pulsation and the significance of its temporal structure have remained elusive. This theoretical study, in combination with biophysical experiments, demonstrates the functional roles of the amplitude and frequency of contraction pulses on epithelial morphogenesis. Although high amplitude pulsing triggers irreversible junction deformation via tension remodeling, junction shortening eventually stalls

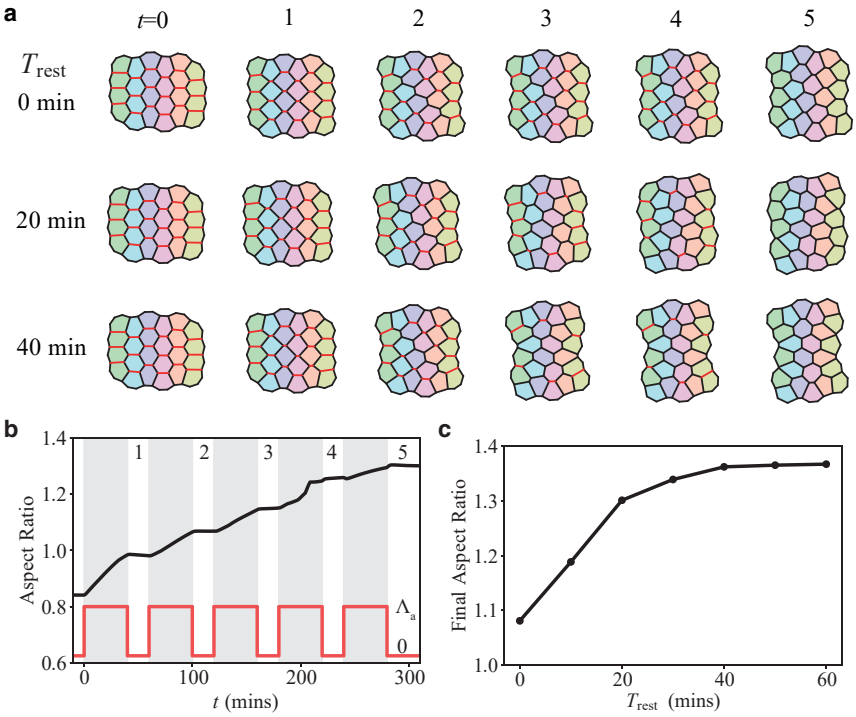

FIGURE 6 Convergence-extension is more effective for longer rest periods between successive activations. Results shown are obtained using the mechanosensitive tension remodeling equations (Eqs. 10 and 11). (*a*) Tissue configurations during five 40-min contractions at different rest periods (T_{rest}) between contractions. Numbers 1–5 indicate the number of rest cycles the tissue has undergone, as shown in (*b*). The cell colors indicate their initial location column-wise, and red edges indicate the initially activated edges. (*b*) Aspect ratio of the tissue versus time, for five 40-min activations (*bottom inset*) with 20 min of rest periods in between. The red pulse shows the applied tension versus time during the activation and rest cycles. (*c*) Final aspect ratio of the tissue versus T_{rest}, showing that longer rest periods promote larger tissue deformation. For parameters see Table 4. To see this figure in color, go online.

for prolonged activation of actomyosin contractility. However, longer rest periods between successive contraction pulses enable a higher degree of junction shortening via mechanical strain relaxation. We show that frequency-dependent modulation of junction deformation, in combination with cell rearrangements, is sufficient to drive tissue-scale shape changes via convergent-extension movements. These results provide a potential new understanding of the significance of pulsatile contractions, suggesting that high amplitude and low frequency myosin pulsing, separated by longer rest periods, is most effective in driving large-scale tissue remodeling via mechanical ratcheting.

Our proposed theory for mechanosensitive epithelial junction remodeling advances the existing cell-based models of epithelial tissues. The widely used vertex model for epithelial mechanics (28), and its existing variants are unable to capture the experimentally measured length dynamics of epithelial junctions upon time-varying contractions. In the vertex model, junctions either contract like a purely elastic material that is reversible upon stress removal or junctions continuously shorten their lengths like a fluid even for a low amount of applied contraction. These predictions are inconsistent with experimental data, where junctions display an elastic behavior only under short or weak activation of RhoA. Longer periods of RhoA activation lead to permanent junction shortening, which saturates for prolonged pulse duration.

To capture the experimental data, we propose a modified vertex model with two essential features of epithelial junction mechanics: thresholded tension remodeling and continuous strain relaxation. In our model, junctions undergo permanent tension remodeling only above a critical strain threshold. This enables irreversible junction deformation for sufficiently strong and prolonged activation of contractility, in agreement with our experimental data. Furthermore, a critical strain threshold for tension remodeling acts as a filter for small amplitude fluctuations in contractile activity, imparting mechanical robustness to the system. However, tension remodeling alone is not sufficient to promote large-scale deformations because junction shortening saturates for prolonged activation of contractility. To this end, continuous strain relaxation in epithelial junctions allows the system to gradually lose memory of its mechanical deformation. As a result, pulsatile activation of contractility with sufficiently long periods of relaxation enables large-scale irreversible deformations in epithelia via ratcheting. Taken together, the combination of mechanosensitive tension remodeling and junctional strain relaxation provides a robust mechanism to guide directed epithelial morphogenesis, as well as enables the maintenance of mechanical homeostasis in epithelial tissues.

TABLE 4 Parameters for Convergence-Extension Simulations

Parameter	Value
Rest length remodeling rate, k_L	0.159 min^{-1}
Critical strain, ε_c	0.122
Initial tension, Y	0.142
tension remodeling rate, k_c	0.020 min^{-1}
tension remodeling rate, k_e	0.000 min^{-1}
Applied contractility, Γ_a	0.085
Friction, μ	1.132 min

SUPPORTING MATERIAL

Supporting Material can be found online at https://doi.org/10.1016/j.bpj.2019.09.027.

AUTHOR CONTRIBUTIONS

S.B., E.M.M., and M.L.G. designed the study. M.F.S. and S.B. developed theory. M.F.S. performed and analyzed simulations. M.L.G. and K.E.C. designed experiments. K.E.C. acquired and analyzed experimental data. M.F.S. and S.B. wrote the manuscript with the help of E.M.M., M.L.G., and K.E.C.

ACKNOWLEDGMENTS

M.F.S. is supported by EPSRC (UK Engineering and Physical Sciences Research Council) funded PhD studentship at University College London. S.B. acknowledges support from the Royal Society (URF/R1/180187) and the Human Frontier Science Program (RGY0073/2018). K.E.C. is supported by a Howard Hughes Medical Institute Gilliam Fellowship, National Academies of Sciences Ford Foundation Fellowship, and NIH training grant (GM007183). M.L.G. acknowledges funding from NIH (RO1 GM104032). E.M.M. acknowledges funding from NIH (RO1 HD099931). The work at University of Chicago was partially supported by the University of Chicago Materials Research Science and Engineering Center, which is funded by the National Science Foundation under award number DMR-1402709.

REFERENCES

1. Martin, A. C., M. Kaschube, and E. F. Wieschaus. 2009. Pulsed contractions of an actin-myosin network drive apical constriction. *Nature.* 457:495–499.
2. Bertet, C., L. Sulak, and T. Lecuit. 2004. Myosin-dependent junction remodelling controls planar cell intercalation and axis elongation. *Nature.* 429:667–671.
3. Heisenberg, C. P., and Y. Bellaïche. 2013. Forces in tissue morphogenesis and patterning. *Cell.* 153:948–962.
4. Levayer, R., and T. Lecuit. 2012. Biomechanical regulation of contractility: spatial control and dynamics. *Trends Cell Biol.* 22:61–81.
5. Lessey, E. C., C. Guilluy, and K. Burridge. 2012. From mechanical force to RhoA activation. *Biochemistry.* 51:7420–7432.
6. Bambardekar, K., R. Clément, …, P. F. Lenne. 2015. Direct laser manipulation reveals the mechanics of cell contacts in vivo. *Proc. Natl. Acad. Sci. USA.* 112:1416–1421.
7. Martin, A. C. 2010. Pulsation and stabilization: contractile forces that underlie morphogenesis. *Dev. Biol.* 341:114–125.
8. Wyatt, T. P., A. R. Harris, …, B. Baum. 2015. Emergence of homeostatic epithelial packing and stress dissipation through divisions oriented along the long cell axis. *Proc. Natl. Acad. Sci. USA.* 112:5726–5731.
9. Khalilgharibi, N., J. Fouchard, …, G. Charras. 2019. Stress relaxation in epithelial monolayers is controlled by the actomyosin cortex. *Nat. Phys.* 15:839–847.
10. Duda, M., N. J. Kirkland, …, Y. Mao. 2019. Polarization of myosin II refines tissue material properties to buffer mechanical stress. *Dev. Cell.* 48:245–260.e7.
11. Clément, R., B. Dehapiot, …, P.-F. Lenne. 2017. Viscoelastic dissipation stabilizes cell shape changes during tissue morphogenesis. *Curr. Biol.* 27:3132–3142.e4.
12. Iyer, K. V., R. Piscitello-Gómez, …, S. Eaton. 2019. Epithelial viscoelasticity is regulated by mechanosensitive E-cadherin turnover. *Curr. Biol.* 29:578–591.e5.
13. Ferro, V., M. Chuai, …, C. Weijer. 2018. Measurement of junctional tension in epithelial cells at the onset of primitive streak formation in the chick embryo via non-destructive optical manipulation. *bioRxiv* https://doi.org/10.1101/501775.
14. Bi, D., J. Lopez, …, M. L. Manning. 2015. A density-independent rigidity transition in biological tissues. *Nat. Phys.* 11:1074–1079.
15. Tetley, R. J., M. F. Staddon, …, Y. Mao. 2019. Tissue fluidity promotes epithelial wound healing. *Nat Phys* Published online August 12, 2019. https://doi.org/10.1038/s41567-019-0618-1.
16. Alt, S., P. Ganguly, and G. Salbreux. 2017. Vertex models: from cell mechanics to tissue morphogenesis. *Philos. Trans. R. Soc. Lond. B Biol. Sci.* 372:20150520.
17. Marée, A. F., V. A. Grieneisen, and P. Hogeweg. 2007. The cellular potts model and biophysical properties of cells, tissues and morphogenesis. *In* Single-Cell-Based Models in Biology and Medicine. A. R. A. Anderson, M. A. J. Chaplain, and K. A. Rejniak, eds. Springer, pp. 107–136.
18. Izaguirre, J. A., R. Chaturvedi, …, J. A. Glazier. 2004. CompuCell, a multi-model framework for simulation of morphogenesis. *Bioinformatics.* 20:1129–1137.
19. Banerjee, S., K. J. Utuje, and M. C. Marchetti. 2015. Propagating stress waves during epithelial expansion. *Phys. Rev. Lett.* 114:228101.
20. Banerjee S., and M.C. Marchetti. Continuum models of collective cell migration, In Cell Migrations: Causes and Functions, C. La Porta and S. Zapperi, eds. (Springer) pp. 45–66.
21. Murisic, N., V. Hakim, …, B. Audoly. 2015. From discrete to continuum models of three-dimensional deformations in epithelial sheets. *Biophys. J.* 109:154–163.
22. Muñoz, J. J., and S. Albo. 2013. Physiology-based model of cell viscoelasticity. *Phys. Rev. E Stat. Nonlin. Soft Matter Phys.* 88:012708.
23. Noll, N., M. Mani, …, B. I. Shraiman. 2017. Active tension network model suggests an exotic mechanical state realized in epithelial tissues. *Nat. Phys.* 13:1221–1226.
24. Curran, S., C. Strandkvist, …, B. Baum. 2017. Myosin II controls junction fluctuations to guide epithelial tissue ordering. *Dev. Cell.* 43:480–492.e6.
25. Bonfanti, A., J. Fouchard, …, A. Kabla. 2019. A unified rheological model for cells and cellularised materials. *bioRxiv* https://doi.org/10.1101/543330.
26. Oakes, P. W., E. Wagner, …, M. L. Gardel. 2017. Optogenetic control of RhoA reveals zyxin-mediated elasticity of stress fibres. *Nat. Commun.* 8:15817.
27. Cavanaugh, K. E., M. F. Staddon, …, M. L. Gardel. 2019. RhoA mediates epithelial cell shape changes via mechanosensitive endocytosis. *bioRxiv* https://doi.org/10.1101/605485.
28. Fletcher, A. G., M. Osterfield, …, S. Y. Shvartsman. 2014. Vertex models of epithelial morphogenesis. *Biophys. J.* 106:2291–2304.
29. Park, J. A., J. H. Kim, …, J. J. Fredberg. 2015. Unjamming and cell shape in the asthmatic airway epithelium. *Nat. Mater.* 14:1040–1048.
30. Nagai, T., and H. Honda. 2009. Computer simulation of wound closure in epithelial tissues: cell-basal-lamina adhesion. *Phys. Rev. E Stat. Nonlin. Soft Matter Phys.* 80:061903.
31. Staddon, M. F., D. Bi, …, S. Banerjee. 2018. Cooperation of dual modes of cell motility promotes epithelial stress relaxation to accelerate wound healing. *PLoS Comput. Biol.* 14:e1006502.
32. Barton, D. L., S. Henkes, …, R. Sknepnek. 2017. Active vertex model for cell-resolution description of epithelial tissue mechanics. *PLoS Comput. Biol.* 13:e1005569.
33. Mao, Y., A. L. Tournier, …, N. Tapon. 2013. Differential proliferation rates generate patterns of mechanical tension that orient tissue growth. *EMBO J.* 32:2790–2803.
34. Farhadifar, R., J.-C. Röper, …, F. Jülicher. 2007. The influence of cell mechanics, cell-cell interactions, and proliferation on epithelial packing. *Curr. Biol.* 17:2095–2104.

35. Schaumann, E. N., M. F. Staddon, …, S. Banerjee. 2018. Force localization modes in dynamic epithelial colonies. *Mol. Biol. Cell.* 29:2835–2847.

36. Brakke, K. A. 1992. The surface evolver. *Exp. Math.* 1:141–165.

37. Strickland, D., Y. Lin, …, M. Glotzer. 2012. TULIPs: tunable, light-controlled interacting protein tags for cell biology. *Nat. Methods.* 9:379–384.

38. Melendez, J., M. Patel, …, M. N. McClean. 2014. Real-time optogenetic control of intracellular protein concentration in microbial cell cultures. *Integr. Biol.* 6:366–372.

39. Odell, G. M., G. Oster, …, B. Burnside. 1981. The mechanical basis of morphogenesis. I. Epithelial folding and invagination. *Dev. Biol.* 85:446–462.

40. McFadden, W. M., P. M. McCall, …, E. M. Munro. 2017. Filament turnover tunes both force generation and dissipation to control long-range flows in a model actomyosin cortex. *PLoS Comput. Biol.* 13:e1005811.

41. Wallingford, J. B., S. E. Fraser, and R. M. Harland. 2002. Convergent extension: the molecular control of polarized cell movement during embryonic development. *Dev. Cell.* 2:695–706.

42. Levine, J. H., Y. Lin, and M. B. Elowitz. 2013. Functional roles of pulsing in genetic circuits. *Science.* 342:1193–1200.

43. Fernandez-Gonzalez, R., and J. A. Zallen. 2011. Oscillatory behaviors and hierarchical assembly of contractile structures in intercalating cells. *Phys. Biol.* 8:045005.

44. Munjal, A., J. M. Philippe, …, T. Lecuit. 2015. A self-organized biomechanical network drives shape changes during tissue morphogenesis. *Nature.* 524:351–355.

45. Michaux, J. B., F. B. Robin, …, E. M. Munro. 2018. Excitable RhoA dynamics drive pulsed contractions in the early *C. elegans* embryo. *J. Cell Biol.* 217:4230–4252.